Estimation of Hurricane Winds From SeaWinds at Ultrahigh Resolution

Brent A. Williams, *Member, IEEE*, and David G. Long, *Fellow, IEEE*

***Abstract*—Although the SeaWinds scatterometer was not specifically designed to observe tropical cyclones, new high-resolution wind products resolve much of the horizontal structure of these storms. However, these higher resolution products (2.5 km) are inherently noisier than the standard 25-km near-surface wind products. These noise levels combined with rain contamination complicate high-resolution wind estimation—particularly in tropical cyclones. Fortunately, tropical cyclones have structures that can be exploited by using a wind field model. This paper develops a new procedure for hurricane wind field estimation from the SeaWinds instrument at ultrahigh resolution. A simplified hurricane model is developed to provide prior information to be used in maximum *a posteriori* probability estimation of ocean winds. Using the hurricane model ameliorates the effects of rain and noise and provides useful hurricane parameters such as the eye center location. The model also improves ambiguity selection. The new method reduces the variability of the wind speed and direction estimates, although high wind speeds still tend to be underestimated. The method also greatly improves wind direction estimates in hurricanes—even in rain-contaminated portions of the storm.**

***Index Terms*—Hurricane, maximum *a posteriori* estimation, scatterometry, wind.**

I. Introduction

DIRECT measurements of wind and rain are difficult to obtain in the extreme conditions of hurricanes. Buoys are often damaged in these intense storms, and ships avoid them. Aircraft radar and dropsonde measurements in hurricanes provide important information, but these data are limited in spatial coverage.

The spaceborne scatterometer SeaWinds has a swath that covers a large region over a short time duration and has provided invaluable data of large-scale global weather. However, the relatively coarse resolution (25 km) of the standard wind product limits its use in resolving small-scale features. Whereas tropical cyclones are apparent in the 25-km product, important storm parameters such as the eye center location are not well resolved.

The dense measurement sampling of the SeaWinds scatterometer makes it possible for the wind to be retrieved at an effective resolution of about 5–7 km and reported on a 2.5-km grid using resolution enhancement techniques [1], [2]. In these ultrahigh resolution (UHR) surface wind data, much of the storm structure of hurricanes is obvious. However, there remain several issues that limit the use of SeaWinds in observing tropical cyclones. Due to the resolution enhancement procedure, the 2.5-km products are inherently noisier than their 25-km counterparts [1]. Tropical cyclones are also associated with heavy rain, which contaminates the wind estimates. Furthermore, the relationship between hurricane force winds and radar backscatter may not be modeled well by the current geophysical model function (GMF), although research is being done to improve the model function for extreme winds [3]. Moreover, the GMF used for the UHR retrievals (QSCAT-1/F13 sometimes termed QMOD3 used by the Jet Propulsion Laboratory (JPL) in standard products) was derived for the 25-km QuikSCAT product [4]. In principle, the GMF should be independent of the resolution. However, because the GMF was derived from QuikSCAT 25-km data, using it for UHR winds may produce somewhat biased results—particularly at very low wind speeds [5], [6].

This paper describes a new method for UHR wind field estimation of tropical cyclones using data from the SeaWinds scatterometer. The focus is primarily to present a new method to improve direction estimates and to reduce the variability of the vector estimates (speed and direction) while preserving mesoscale detail. A simple low-order hurricane wind field model is developed to provide prior information for maximum *a posteriori* probability (MAP) estimation of the wind. Using the hurricane model ameliorates the effects of rain and noise. The new method provides improved ambiguity selection, alternate wind estimates (MAP ambiguities), and estimates of important hurricane parameters. Simulation is employed to explore the effects of rain on the new method. The accuracy of the hurricane model parameter estimates is analyzed by using the best track hurricane eye locations provided by the National Hurricane Center (NHC) and the interpolated numerical weather prediction (NWP) winds provided by the National Centers for Environmental Prediction (NCEP). The quality of the wind field estimates is analyzed by using H*Winds made available by NOAA's Hurricane Research Division [7].

This paper is organized as follows. Section II reviews the pertinent principles of scatterometry and the high-resolution wind products derived form SeaWinds. Section III outlines the new MAP wind estimation procedure for hurricanes. Section IV develops the hurricane wind field model appropriate for scatterometry. Section V describes a simplification of the new method that allows for near real-time implementation. Section VI analyzes the quality of the results. Section VII concludes.

Manuscript received September 13, 2007; revised March 5, 2008. Current version published October 1, 2008.

B. A. Williams is with the Electrical and Computer Engineering Department, Brigham Young University, Provo, UT 84602 USA.

D. G. Long is with the Electrical and Computer Engineering Department and the Center for Remote Sensing, Brigham Young University, Provo, UT 84602 USA.

Color versions of one or more of the figures in this paper are available online at http://ieeexplore.ieee.org.

Digital Object Identifier 10.1109/TGRS.2008.924096

II. Principles of Scatterometry

This section reviews the principles involved in scatterometry. Pertinent information about the SeaWinds design is also provided.

SeaWinds measures the radar backscatter, which is denoted as σ^0, from the Earth's surface. Over the ocean, σ^0 is related to the wind speed and direction through the GMF. Measurements from multiple azimuth angles are necessary to estimate the wind direction. SeaWinds makes four different types of measurements, vertical and horizontal polarization beams each with a fore and aft look, which provide several samples from different azimuth angles for each resolution cell. Because the v-pol and h-pol beams have different incidence angles, the outer portion of the swath is only illuminated by one beam [8].

Conventionally, the wind is estimated in two steps. First, the maximum-likelihood (ML) estimation of the wind from the σ^0 measurements is performed for each resolution or wind vector cell. Because the ML objective function is multimodal due to the double cosine dependence of the GMF on wind direction, ML estimation results in multiple wind vector solutions (ambiguities). The second step requires the selection of the appropriate ambiguity. Although there exist more sophisticated ambiguity selection algorithms, the standard L2B product uses a simple one. For the standard 25-km product (L2B), the ambiguities closest to NWP winds are selected (a procedure known as nudging) and then a spatial median filter is used to select the final ambiguities [9]. Alternatively, the DIRTH ambiguity selection routine is used in standard JPL processing [10].

High-resolution σ^0 fields are obtained by separately applying image reconstruction to each of the four types of σ^0 measurements. This provides four separate σ^0 fields with regularly spaced samples. Wind retrieval is then performed for each high-resolution cell, producing high-resolution wind ambiguities. High-resolution ambiguity selection is problematic because the NWP winds used in ambiguity selection poorly represent small-scale features. Ambiguity selection is further complicated by rain contamination and increased noise level. The current UHR wind product retrieves the wind based on an ML estimation scheme and selects the ambiguities closest to the L2B vectors, which are then median filtered.

In tropical cyclones, the UHR product can resolve structure that is not apparent in the 25-km product. The eye center location, rain bands, and mesoscale convective events are resolved in the high-resolution wind speed field. The resolution of the direction field, however, is limited by the nudging field in conventional ambiguity selection.

III. MAP Estimation for Tropical Cyclones

The wind estimation method presented here takes a novel approach. A low-order hurricane model is developed and used as the mean of a fieldwise prior distribution of the wind. This prior distribution is used to augment the ML objective function-producing MAP ambiguities and the fieldwise MAP estimate of the wind. In the sequel, we also develop a method based on MAP estimation to improve the ambiguity selection of the pointwise ML ambiguities.

This section explains the theory behind the MAP estimation method. First, an overview of pointwise MAP estimation and ML estimation is provided. Then, fieldwise MAP estimation using the hurricane model is developed. Next, the new method is contrasted with the conventional model-based and pointwise approaches.

A. Pointwise MAP Estimation

In contrast to conventional pointwise ML wind estimation, which finds the wind vector that maximizes the probability of σ^0, given the wind speed and direction $P(\sigma^0|S,D)$, pointwise MAP estimation maximizes the probability of the vector wind, given the σ^0 measurements $P(S,D|\sigma^0)$. This probability distribution can be found using Bayes' rule

$$\begin{aligned} P(S,D|\sigma^0) &= \frac{P(\sigma^0,S,D)}{P(\sigma^0)} \\ &= \frac{P(\sigma^0|S,D)P(S,D)}{P(\sigma^0)} \\ &= \frac{1}{P(\sigma^0)}\text{ML} \times \text{PRIOR} \end{aligned} \tag{1}$$

where the probability distribution $P(S,D)$ is the prior distribution of the wind. The MAP objective function $P(S,D|\sigma^0)$ is essentially a weighted version of the ML objective function $P(\sigma^0|S,D)$. Given the multiple σ^0 measurements, the wind speed and direction that maximize $P(S,D|\sigma^0)$ can be found.

The pointwise ML objective function represents a joint distribution of independent Gaussian random variables and has the form [11]

$$P(\sigma^0|S,D) = \prod_i \frac{1}{\sqrt{2\pi}\xi_i} e^{-\frac{\left(\sigma_i^0 - \mathcal{M}_i(S,D,\ldots)\right)^2}{2\xi_i^2}} \tag{2}$$

where σ_i^0 represents the ith σ^0 measurement, $\mathcal{M}_i(S,D,\ldots)$ represents the σ^0 value resulting from projecting the given wind vector through the GMF with the same measurement geometry as the ith measurement, and ξ_i is a variance term that is a function of the measurement noise and the modeling uncertainty of the GMF. Therefore, if the pointwise prior distribution is known, the pointwise MAP estimate can be found by scaling the ML objective function by $P(S,D)$ and searching for the maxima. Note that $P(\sigma^0)$ represents the probability distribution of σ^0 and is not a function of S and D, which are to be estimated. Thus, it can be factored out of the maximization. This produces the pointwise wind vector estimate

$$\begin{aligned} \{\hat{S},\hat{D}\} &= \arg\max_{S,D} \left\{P(\sigma^0|S,D)P(S,D)/P(\sigma^0)\right\} \\ &= \arg\max_{S,D} \left\{P(\sigma^0|S,D)P(S,D)\right\}. \end{aligned} \tag{3}$$

B. Fieldwise MAP Estimation

For fieldwise estimation, the entire wind speed field $\bar{S}$ and direction field $\bar{D}$ are estimated. The fieldwise prior distribution $P(\bar{S},\bar{D})$ is given by the hurricane model. For each resolution cell, the speed and direction are assumed to be independent

Gaussian random variables with means given by the model and some variance. Using this construction, the prior distribution for one cell has the form

$$\begin{aligned} P(S,D) &= P(S)P(D) \\ &= \frac{1}{\sqrt{2\pi}\xi_S} e^{-\frac{(S-\mathcal{S})^2}{2\xi_S^2}} \frac{1}{\sqrt{2\pi}\xi_D} e^{-\frac{(D-\mathcal{D})^2}{2\xi_D^0}} \end{aligned} \tag{4}$$

where $\mathcal{S}$ and $\mathcal{D}$ are the speed and direction of the hurricane model wind for the resolution cell of interest, respectively. This construction provides prior distributions for each resolution cell.

The notion of correlation between adjacent cells is captured by the similarity of the means of the prior distributions rather than the imposition of a correlation between the distributions (i.e., the distributions are statistically independent although the means of the distributions are linked by the fieldwise model). This allows for the small-scale variability and preservation of high-frequency information although this may preserve high-frequency noise as well. Assuming correlation between adjacent cells imposes additional structure on the estimated wind field. Because we desire estimates that are based primarily on the measurements and only moderately impacted by the model (because the model is simplistic), assuming independence between adjacent cells is appropriate for this application. Nevertheless, a more sophisticated model allowing a correlation between adjacent cells may produce a more accurate result.

Independence between the distributions of adjacent resolution cells causes the fieldwise prior to be equal to the product of the pointwise priors, $P(\bar{S},\bar{D}) = \prod_{m,n} P(S,D)$. Assuming that each resolution cell is independent from each other also enables the fieldwise ML objective function to be written as the product of the pointwise objective functions. Thus, the fieldwise MAP objective function has the form

$$\begin{aligned} P(\bar{S},\bar{D}|\bar{\sigma}^0) &= \frac{1}{P(\bar{\sigma}^0)} P(\bar{\sigma}^0|\bar{S},\bar{D}) P(\bar{S},\bar{D}) \\ &= \frac{1}{P(\bar{\sigma}^0)} \prod_{m,n} \left\{ P(S)P(D) \prod_i P\left(\sigma_i^0|S,D\right) \right\} \\ &= \frac{1}{P(\bar{\sigma}^0)} \prod_{m,n} \left\{ \frac{1}{2\pi\xi_S\xi_D} e^{\frac{-(S-\mathcal{S}(\bar{\alpha}))^2}{2\xi_S^2}} e^{\frac{-(D-\mathcal{D}(\bar{\alpha}))^2}{2\xi_D^2}} \right. \\ &\qquad \left. \times \prod_i \frac{1}{\sqrt{2\pi}\xi_i} e^{-\frac{\left(\sigma_i^0-\mathcal{M}_i\right)^2}{2\xi_i^2}} \right\} \end{aligned} \tag{5}$$

where $\bar{\sigma}^0$, $\bar{S}$, and $\bar{D}$ represent the σ^0, wind speed, and wind direction fields of the study region, respectively. σ_i^0, S, and D represent the ith σ^0 measurement, the wind speed, and the wind direction, respectively, for a particular resolution cell at index (m,n) of the fields. Also, $\mathcal{S}(\bar{\alpha})$ and $\mathcal{D}(\bar{\alpha})$ represent the hurricane model speed and direction, respectively, for a cell at index (m,n), where $\bar{\alpha}$ represents a vector of hurricane model parameters.

Note that (5) states that the fieldwise MAP objective function is a scaled product of the pointwise objective functions of each cell in the fieldwise grid. Likewise, it can be shown that, with this construction, the fieldwise MAP value is a scaled product of the pointwise MAP values for a particular model instance

$$\begin{aligned} \text{MAP}_{\text{fw}} &= \max_{\bar{S},\bar{D}} P(\bar{S},\bar{D}|\bar{\sigma}^0) \\ &= \max_{\bar{S},\bar{D}} \frac{1}{P(\bar{\sigma}^0)} \prod_{m,n} \left\{ P(S)P(D) \prod_i P\left(\sigma_i^0|S,D\right) \right\} \\ &= \frac{1}{P(\bar{\sigma}^0)} \prod_{m,n} \max_{S,D} \left\{ P(S)P(D) \prod_i P\left(\sigma_i^0|S,D\right) \right\} \\ &= \frac{1}{P(\bar{\sigma}^0)} \prod_{m,n} \text{MAP}_{\text{pw}}. \end{aligned} \tag{6}$$

The best model instance is the one that maximizes the fieldwise MAP value. Thus, the fieldwise MAP value becomes the hurricane model objective function

$$l = \max_{\bar{\alpha}} \left\{ \text{MAP}_{\text{fw}}(\bar{\alpha}) \right\}. \tag{7}$$

For practical implementation, the log of the fieldwise objective function is maximized. Taking the log of (5), leaving out constant terms, and then maximizing over wind fields and hurricane model parameters produces

$$\begin{aligned} L = \max_{\bar{\alpha}} \left\{ \sum_{m,n} \max_{S,D} \left\{ \frac{-(S-\mathcal{S}(\bar{\alpha}))^2}{\xi_S^2} - \frac{(D-\mathcal{D}(\bar{\alpha}))^2}{\xi_D^2} \right.\right. \\ \left.\left. - \sum_i \frac{\left(\sigma_i^0 - \mathcal{M}(S,D)\right)^2}{\xi_i^2} \right\} \right\}. \end{aligned} \tag{8}$$

The arguments S, D, and $\bar{\alpha}$ that maximize the log likelihood value L are the estimates of the wind speed and direction for each resolution cell and the hurricane model parameters. This method simultaneously estimates the hurricane model parameters and the wind field. Note that, if we factor out a negative sign from the right side of (8), the objective function must be searched for minima rather than maxima and we obtain an expression similar to the standard ML objective function. The expression in (8) is similar to procedures frequently used in NWP data assimilation [12], [13]. However, the measurement term (the last term on the right) remains Gaussian in the σ_0 domain, which is consistent with standard ML wind retrieval schemes. We note that certain wind directions may be favored for certain measurement geometries by the MLE objective function [14]. This may also be inherited by the MAP estimator described here.

C. Implications

The new approach diverges from conventional model-based methods. Here, model-based implies using a fieldwise model to describe the 2-D structure of the surface vector wind. Conventional model-based methods estimate only the parameters of the wind field model. These methods force the wind estimate to be in the space spanned by the model. Thus, the resulting wind fields only contain information captured by the model. For a practical low-order model, forcing the wind field estimate to be in the space spanned by the model restricts the wind field

estimates to low resolution. The new MAP construction allows for the preservation of the information that is obtainable by a nonmodel-based approach (pointwise ML estimation) while emphasizing the structure described by the model.

The difference between the pointwise ML, model-based fieldwise ML, and fieldwise MAP estimations is illustrated by the following. All three of these methods can be formulated as a constrained optimization problem. For pointwise ML estimation, the problem statement is as follows:

For each cell at index (m, n)
maximize
$$\sum_i \frac{-\left(\sigma_i^0 - \mathcal{M}(S, D)\right)^2}{\xi_i^2}$$
$$\left[\text{or equivalently } P(\sigma^0|S, D)\right]$$
subject to
$$S \geq 0 \text{ and } 0 < D \leq 360.$$

This produces up to four possible wind ambiguities for each resolution cell due to the local maxima in the objective function. Ignoring ambiguities (only considering the absolute maxima that corresponds to the first ambiguity), the pointwise objective functions can be summed up to form a fieldwise objective function. The pointwise ML estimation problem statement for the entire field (fieldwise ML estimation) can thus be written as

maximize
$$\sum_{m,n,i} \frac{-(\sigma_i^0 - \mathcal{M}(S, D))^2}{\xi_i^2}$$
$$\left[\text{or equivalently} P(\bar{\sigma^0}|\bar{S}, \bar{D})\right]$$
subject to
$$S \geq 0 \text{ and } 0 < D \leq 360 \text{ for all } (m, n)$$

because both problem statements result in the same wind field. This can be interpreted as a fieldwise objective function that is maximized when the pointwise objective function of each resolution element is maximized. Such a result allows comparisons of pointwise with fieldwise techniques. For model-based ML estimation with the assumption that each resolution element is independent, the problem statement can be expressed as

maximize
$$\sum_{m,n,i} \frac{-(\sigma_i^0 - \mathcal{M}(S, D))^2}{\xi_i^2}$$
$$[\text{or equivalently } P(\bar{\sigma}^0|\bar{S}, \bar{D})]$$
subject to
$$\bar{S} = \mathcal{S}(\bar{\alpha}), \bar{D} = \mathcal{D}(\bar{\alpha})$$
$$\text{where } S\epsilon\bar{S} \text{ and } D\epsilon\bar{D}.$$

This is equivalent to estimating the model parameters $\bar{\alpha}$ and then generating the estimate of the wind field using the model. The fieldwise and model-based ML estimation methods optimize the same metric but the model-based ML estimation method restricts the solution space more than the pointwise ML estimation method. The fieldwise MAP estimation method searches the same solution space as the fieldwise ML estimation method but optimizes an augmented metric. For fieldwise MAP estimation, the problem statement is as follows:

maximize
$$\sum_{m,n,i} \left\{ \frac{-\left(S - \mathcal{S}(\bar{\alpha})\right)^2}{\xi_S^2} - \frac{\left(D - \mathcal{D}(\bar{\alpha})\right)^2}{\xi_D^2} - \frac{\left(\sigma_i^0 - \mathcal{M}\left(S, D\right)\right)^2}{\xi_i^2} \right\}$$
$$\left[\text{or equivalently } P(\bar{S}, \bar{D}|\bar{\sigma}^0)\right]$$
subject to
$$S \geq 0 \text{ and } 0 < D \leq 360 \text{ for all } m, n.$$

The fieldwise MAP estimation approach can be viewed as pointwise MAP estimation with priors given by a fieldwise model. Remember that ξ_i characterizes the uncertainty of the ith observation of the true σ^0. If the variance terms ξ_S and ξ_D are very large compared to the ξ_i's, the fieldwise MAP objective function effectively becomes the fieldwise ML objective function. Furthermore, if ξ_S and ξ_D are small compared to the ξ_i's, any solution that is not in the space spanned by the hurricane model produces a large and negative MAP value (in log space) and the fieldwise MAP problem statement essentially becomes equivalent to the model-based ML estimation problem statement. Thus, the variance terms control how much the hurricane model is imposed. The relative values between ξ_S, ξ_D, and ξ_i are measures of the importance of the model speed error, the model direction error, and the actual measured σ^0 error, respectively. ξ_i is a function of the measurement and the true wind, whereas ξ_S and ξ_D are linked to the hurricane model. Furthermore, ξ_S and ξ_D can be scaled relative to the ξ_i's in order to minimize the influence of the hurricane model while maintaining an acceptable noise level (variability of the estimates). Nominal values of ξ_S and ξ_D are empirically found in the sequel.

Imposing a prior on the wind has positive consequences as well as limitations. The new method ameliorates the cross-track pinning of the winds caused by rain and simplifies, or even eliminates, the issue of ambiguity removal. However, the priors modify the ML objective function so that the resulting estimates are no longer "pure" measurements (they are combinations of measurements and a model). Nevertheless, the MAP estimation method imposes the hurricane model less severely than true model-based estimation.

IV. Empirical Hurricane Model

This section develops the empirical hurricane model that provides the prior distributions for the MAP estimation wind retrieval procedure. The model is not dynamic but is rather a simple "snapshot" model of the horizontal structure of the near-surface winds of hurricanes. First, the statistics of real storms are analyzed and empirical distributions are developed from high-resolution SeaWinds wind data. Although these winds are rain contaminated and may contain ambiguity selection errors, we assume that these effects average out. Nevertheless, we recognize that there may still remain a bias in the estimates due to rain effects [15], [16]. We neglect this issue

here so that the model is consistent with the standard GMF used in wind retrieval. Using scatterometer data to derive the model produces a model that is consistent with and appropriate for the scatterometer data.

Although the model developed is simplistic, the MAP estimation and ambiguity selection procedures can be scaled to impose the model as weakly (or strongly) as desired. Thus, the benefits of imposing the large-scale structure described by the model are obtained, whereas the small-scale structure that is not described by the model is preserved.

We hypothesize that much of the asymmetrical structure of the storms can be described by a superposition of a mean wind flow (mean flow) through the region containing the storm [3]. This hypothesis is tested and verified by orienting the storms according to this mean flow and then generating new empirical distributions for the wind speed and direction. This asymmetry is then further investigated by binning the storms by the size and magnitude of the mean flow and generating empirical distributions for each type of storm. Finally, a model is developed based on the relationship between the size of the storm and the mean flow.

A. *Empirical Distribution of Hurricane Winds*

Empirical probability density functions (pdfs) for the priors are obtained by using QuikSCAT-derived conventional high-resolution data of a large number (100) of observations of named storms in the North Atlantic Basin from 1999 to 2005. Normalized histograms (empirical pdfs) are generated by binning the wind speeds and directions as a function of distance from the eye (1 km per bin). The direction relative to the eye center (relative direction) is defined as the angle between the eye vector (the vector drawn from the eye center to the resolution cell of interest) and the wind vector in a clockwise manner from the eye vector.

Note that, in generating the empirical priors, we include all UHR retrieved wind estimates with only minimal use of quality control. Quality control methods are important to ensure the reliability of the hurricane model as well as the resulting estimates. As a quality control metric, high-resolution simultaneous wind and rain retrievals may be used to throw out rain-contaminated winds. Several low-resolution quality control methods have proven effective for use in 25-km products [17], [18]. However, the effectiveness of using low-resolution quality control for use with the UHR products as well as within hurricanes has yet to be explored. Furthermore, low-resolution quality control methods tend to flag large portions of hurricanes as poor due to rain and uncertainty in the GMF. Discarding these data limits the amount of data needed to derive the prior distributions as well as fit the hurricane model in the wind retrieval step. Other limitations include the fact that the QMOD3 GMF tends to underestimate very high wind speeds. This produces a hurricane wind field model whose high wind speeds may also be underestimated. This issue may be corrected by using bias correction post wind retrieval or by improving the GMF. However, due to lack of truth data and because we are primarily concerned with improving direction estimates, neither bias correction nor GMF adjustment is employed.

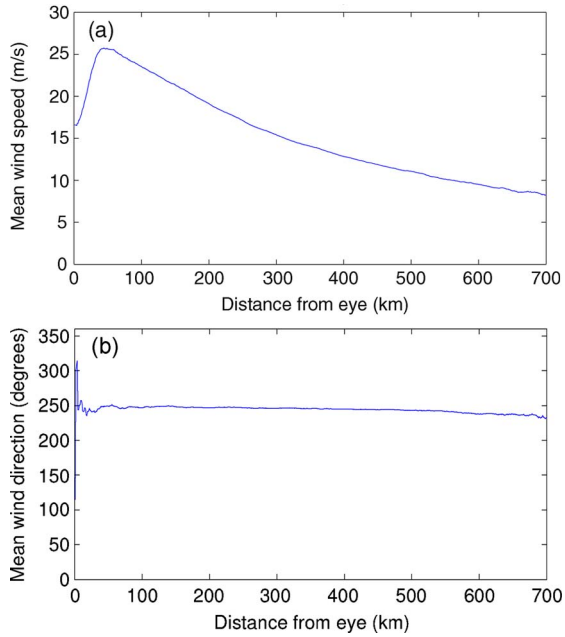

Fig. 1. Means of the empirical speed and relative direction distributions as a function of distance from the hurricane eye. (a) Mean of the wind speed distribution. (b) Mean of the relative direction distribution.

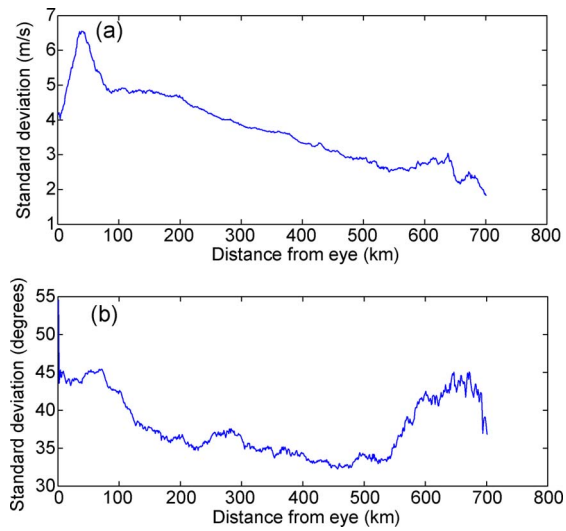

Fig. 2. Standard deviations of the empirical speed and relative direction distributions as a function of distance from the hurricane eye. (a) Standard deviation of the wind speed distribution. (b) Standard deviation of the relative direction distribution.

Fig. 1 shows the mean of the wind speed and direction relative to the eye center as a function of distance from the eye center. The mean of the direction distribution is about 250° rather than 270°, which produces vectors that are orthogonal to the vector drawn from the eye center to the resolution cell of interest. This is consistent with the known fact that there is a significant degree of convergence (negative divergence) in the near-surface wind fields of hurricanes.

Fig. 2 shows the standard deviations of the scatterometer wind speed and direction as a function of distance from the eye. The peak near the eye center of the standard deviation of the direction distribution is caused by several factors including rain contamination, ambiguity selection errors, artifacts of

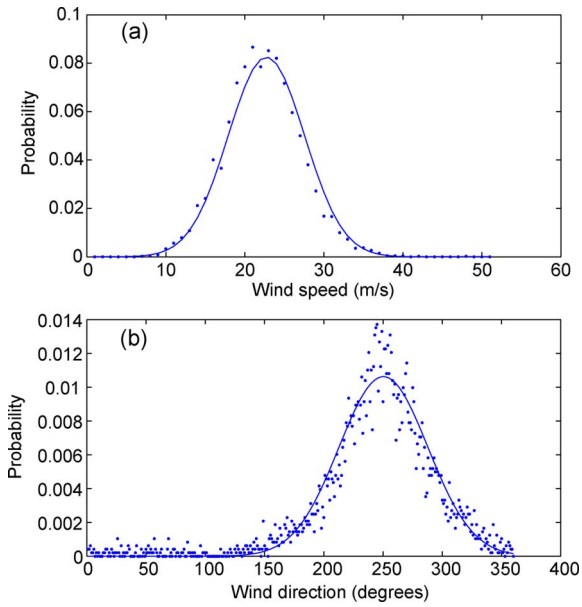

Fig. 3. Wind speed and relative direction distributions for a particular distance from the eye center (140 km) with a Gaussian fit superimposed. (a) Wind speed distribution. (b) Relative wind direction distribution. Both distributions are similar to the Gaussian, suggesting that a Gaussian approximation can be used.

small-scale features, and insufficient data for the statistics to converge. The higher standard deviation that is far from the eye can be attributed to the lack of data and to other convective events outside the immediate vicinity of the hurricane center.

Fig. 3 shows a plot of the empirical distributions for the wind speed and direction for a particular distance from the eye (140 km) with a Gaussian fit superimposed. Although the direction distribution may have some significant higher order moments, both the wind speed and direction distributions are similar to the Gaussian distributions. This justifies the Gaussian approximation used in the development of the MAP estimation procedure in Section III.

B. Investigating Asymmetry

The empirical distributions developed previously describe the bulk structure of the storms as a function of distance from the eye. The asymmetrical structure of the storms is now investigated by using an empirical approach.

The same 100 named storms are oriented so that the mean flow is pointed in the same direction. Then, a histogram is generated where the wind is binned with respect to the angle from mean flow as well as the distance from the eye center. The mean flow is determined by the vector mean of the wind field (care is taken to include the same number of vectors on each side of the eye to suppress a bias in the mean).

Fig. 4 shows the mean of the wind speed as a function of the angle from the mean flow for several distances from the eye center. The curve shows the asymmetry due to the mean flow. The peak near the 90° bin shows that the right side of the storm, with respect to the direction of the mean flow, tends to have the highest wind speed. Fig. 5 shows the standard deviation of the wind speed as a function of distance from the eye averaged over several angles from the mean flow (dashed line) as well as the standard deviation without taking the mean flow into account

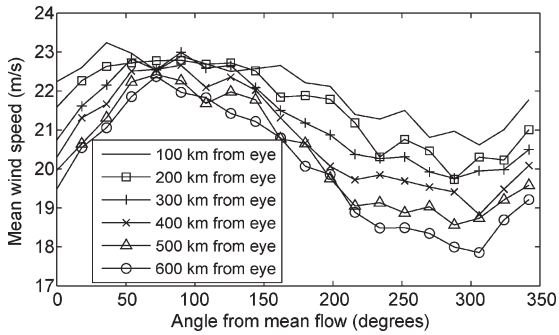

Fig. 4. Mean of the wind speed distribution as a function of angle from mean flow for various distances from the hurricane eye. This pattern affirms that the right side of the storm (with respect to the mean flow) generally has a higher wind speed than the left side.

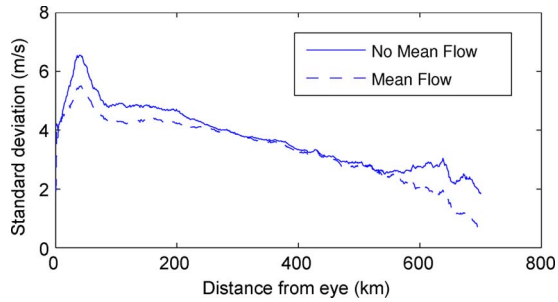

Fig. 5. Standard deviation of the empirical wind speed distribution versus distance from the eye averaged over several angles from mean flow. The upper line is the standard deviation without taking the mean flow into account.

(solid line). The standard deviation is generally reduced when taking the mean flow into account. This implies that the superposition of a mean wind flow can be used to describe the general flow in a hurricane better than a pure axially symmetric field.

Further analysis is employed in order to investigate the relationship between the magnitude of the mean flow, size, and asymmetrical structure of a storm. Each storm is binned according to its size and the magnitude of the mean flow. Then, the storms are oriented so that the direction of the mean flow is the same and speed and direction histograms are generated for each resolution cell on the new grid (oriented according to the eye center and mean flow). The size of the storm is determined by the root mean square (rms) value of the speed in a region including all cells within 150 km from the eye. The means and standard deviations of the wind speed and direction distributions are also calculated. The plots in Fig. 6 show the slices of the mean wind speeds for large and small storms with various magnitudes of the mean flow. A storm is considered small (or large) if the rms speed near the eye is less than or equal to 22 m/s (or greater than 22 m/s). Mean flow is categorized as low, medium, or high if the magnitude of the vector mean is less than or equal to 2.5 m/s, greater than 2.5 m/s and less than or equal to 5 m/s, or greater than 5 m/s, respectively. The slices that are orthogonal to the mean flow are reported because they represent the most extreme asymmetry due to the mean flow. The large and small storms have similar speed profiles but the large storm speeds are scaled higher. Also, the left side of the storm (with respect to the mean flow) is generally less intense than the right side and the asymmetry is increased with a higher magnitude of the mean flow.

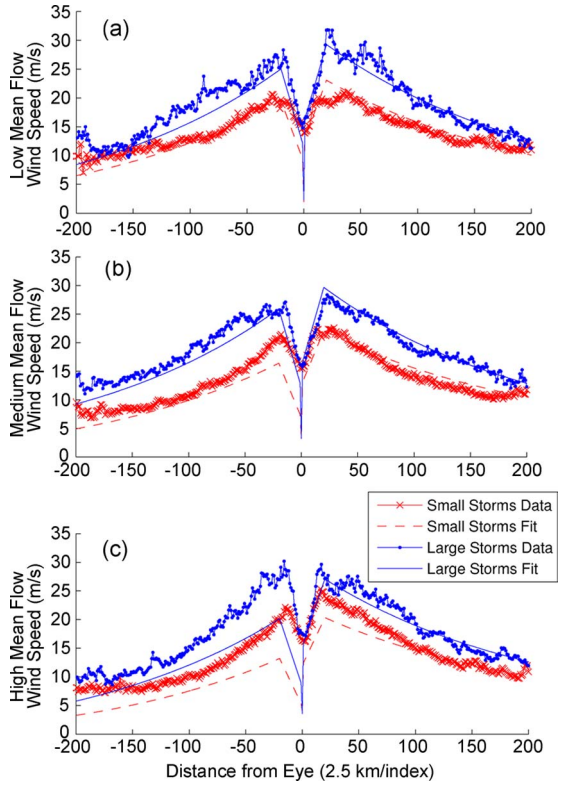

Fig. 6. Slices of the mean of the empirical wind speed distributions orthogonal to the mean flow vector for large and small storms with various magnitudes of the mean flow. (a) Low mean flow. (b) Medium mean flow. (c) High mean flow. The corresponding speed profiles from the simplified hurricane model are superimposed.

C. Hurricane Model

Any of the empirical distributions previously described can be used directly in the MAP wind retrieval process; however, this section develops a simple model that approximates the empirical distribution where the mean flow and storm size are taken into account. This allows interpolation between the coarsely binned sizes of storms and mean flows of the empirical distributions. A simplistic model with few parameters is developed to describe the large-scale horizontal structure of the near-surface winds of a hurricane as a function of the hurricane size and the mean flow (and eye center location). The model assumes that the hurricane wind field is composed of a symmetric cyclonic wind field with a superimposed mean wind flow.

To obtain the structure of the wind field, a simple curve is fit to the speed profile in Fig. 1. This simple curve ramps up linearly from about half of the maximum speed to the maximum speed and then falls off exponentially to a mean offset. For simplicity, we assume a mean offset which is constant over all types of hurricanes. Using the curve in Fig. 1, we choose a mean offset of 7 m/s (which is also approximately the mean wind speed over the ocean). Fitting this curve to the speed profile in Fig. 1 provides nominal values for the radius of maximum wind speed of the eye and the decay rate of the exponential portion. This produces a radius of maximum wind speed of about 50 km and a spatial decay rate of about 475 km. A model realization is generated by producing a symmetric cyclonic wind field with the appropriate speed profile and direction field (250° from eye vector) and by superimposing a mean wind flow.

TABLE I
VECTOR RMS DIFFERENCES BETWEEN THE MEAN OF THE EMPIRICAL DISTRIBUTIONS AND THE MODEL FIT FOR LARGE AND SMALL STORMS WITH VARIOUS MAGNITUDES OF MEAN FLOW

	Mean Flow		
	Low	Medium	High
Small Storms	3.05 m/s	2.97 m/s	5.31 m/s
Large Storms	4.39 m/s	5.00 m/s	7.07 m/s

The plots in Fig. 6 show the slices of the speed fields of the hurricane model fits as well as the mean wind speeds for large and small storms with various magnitudes of the mean flow. The model fits for low and medium wind flow match the data well, but the fit for the high mean flow shows slightly more asymmetry than what the data suggest. This is due to lack of high mean flow cases, which are more rare. For these cases, the rain contamination and ambiguity selection errors may not have been averaged out.

Table I shows the vector rms differences between the means of the empirical speed and direction distributions and the model fit for large and small storms with various magnitudes of the mean flow for the same North Atlantic storms. As expected, the high mean flow case has larger rms differences than the other two cases; however, all the cases have a relatively low rms difference (less than 7.1 m/s), suggesting that the model fits the mean of the empirical distributions well. Thus, the model may be used to describe the storm structure with respect to its size and mean flow.

With these results in mind, the means for the prior distributions for MAP estimation are derived from the simplified hurricane model fit to the data (in the sense of optimizing the MAP objective function). This provides the estimates of the eye center location (latitude and longitude), the magnitude and direction of the mean flow vector, and the maximum speed scale factor, which are the parameters of the hurricane model. The variances of the priors are obtained from the general empirical distributions in Fig. 2. We conservatively assume that the standard deviation of the speed and direction are constant at 7 m/s and 45°, respectively.

V. IMPLEMENTATION

Incorporating the prior described in Section IV into the MAP estimation procedure requires the search of a nonlinear objective function of several variables (the hurricane parameters as well as the wind speed and direction at each resolution cell). This is computationally taxing and can be a deterrent for using such a method in near real-time processing. This section considers a simplification by constraining the solution space to that spanned by the pointwise ambiguities (MAP ambiguity selection). This reduces the search space considerably, as well as produces an estimate of the wind that is not biased by the model. This section also considers the estimation of the eye center from the speed field before performing MAP ambiguity selection, which reduces the search space even further.

MAP ambiguity selection is performed to reduce computation and to provide an improved ML estimate of the wind. MAP ambiguity selection is a form of weak nudging. Instead of forcing the ML ambiguity choice to be closest to the nudging field, MAP ambiguity selection allows for the likelihood value

to dominate the speed and direction error—thus, the ambiguity with the higher probability will be chosen more often than with conventional nudging. This new fieldwise MAP ambiguity selection procedure begins with conventional high-resolution pointwise estimation. The ambiguities are then chosen to maximize the log of the fieldwise MAP objective function. Thus, (8) becomes

$$L^* = \max_{\bar{\alpha}} \left\{ \sum_{m,n} \max_{k} \left\{ \frac{-(S_k - \mathcal{S}(\bar{\alpha}))^2}{\xi_S^2} - \frac{(D_k - \mathcal{D}(\bar{\alpha}))^2}{\xi_D^2} - \sum_i \frac{\left(\sigma_i^0 - \mathcal{M}(S_k, D_k)\right)^2}{\xi_i^2} \right\} \right\} \quad (9)$$

where S_k and D_k are the speed and direction of the kth pointwise ambiguity, respectively. This fieldwise MAP ambiguity selection procedure produces estimates of the hurricane model parameters as well as the selection of appropriate ambiguities. Fieldwise MAP ambiguity removal is not MAP wind retrieval. Ambiguity selection cannot provide the same immunity to rain and noise that is possible with MAP wind retrieval. Nevertheless, MAP ambiguity selection is useful in two ways. First, it can provide an estimate of the wind that is not biased by the model. Second, performing fieldwise MAP ambiguity selection provides estimates of the hurricane model parameters that can be used in MAP wind retrieval. Performing MAP estimation with these hurricane model parameters is more computationally efficient than simultaneously estimating the wind and the hurricane model parameters. Thus, fieldwise MAP estimation (or wind retrieval) can also be done in near real time, and the fieldwise MAP ambiguity selection (of the ML ambiguities) is also provided.

Although MAP ambiguity selection reduces the search space significantly, the method remains computationally taxing. To simplify the problem further, a method for finding the eye center from the first ambiguity speed field before applying MAP ambiguity selection is developed. This method is based on the circular Hough transform (CHT). The CHT is used to find circles in a binary image (an image consisting of ones and zeros). If the radius R of the circle is known, the CHT is calculated simply by drawing a circle of radius R from each pixel that has a value of one in the binary image and accumulating the number of these circles that hit each pixel. Thus, the maximum value of the CHT is at the same index as the center point of the circle. For finding the hurricane eye, the speed field is converted to a binary image and then searched for a circle with a 50-km radius. Then, the CHT is weighted by the inverse of the speed field. This suppresses circle centers in high wind speed regions and emphasizes those in low wind speed regions (like the eye center). Finally, the index of the maximum of the weighted CHT is reported as the hurricane eye center. We note that when the eye is over land or outside the swath, the CHT method produces erroneous eye center estimates. We also note that there may be several local maxima in the weighted CHT. The other local maxima typically occur in heavy rain bands (because rain attenuation may cause the rain bands to appear as lower wind speeds), but because these are not typically circular, the CHT value of the true eye tends to dominate.

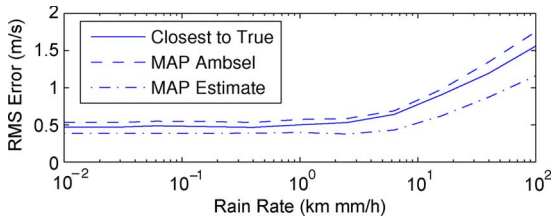

Fig. 7. RMS error versus rain rate for ideal ambiguity selection, MAP ambiguity selection, and MAP estimation.

VI. Analysis

It is difficult to validate the MAP estimation method for hurricanes because truth data are limited—particularly in spatial coverage. One indicator of the quality of the result is the accuracy of the estimates of the hurricane model parameters. Another is the accuracy of the estimated wind. In this section, simulation is employed to explore the effect of rain on MAP estimation and MAP ambiguity selection. Also, the new eye center estimates are compared to the best track locations provided by the NHC. Interpolated NCEP winds are used to check the quality of the other estimated hurricane model parameters (the mean flow and maximum speed scale factor). Although, NCEP winds are limited in resolving fine scale hurricane structure, they may be used as an indicator of consistency of the estimated mean flow and maximum speed scale factor parameters. Finally, the H*Wind hurricane model winds provided by NOAA's Hurricane Research Division [7] are used to check the quality and integrity of the estimated winds. The H*Wind products are smoothed over several hours, and although they are reported with a grid spacing of about 5–6 km, the actual resolution is much more coarse than the UHR winds. Nevertheless, they portray the large-scale structure of hurricanes well.

A. Simulation

Simulation is employed to analyze the effectiveness of the new approach. Synthetic σ^0 values are generated by projecting H*Wind wind fields and synthetic uniform rain rates through the simultaneous wind and rain model described by Draper and Long [19] and by adding Monte Carlo noise. The noise represents communication noise ν and is modeled by a zero mean Gaussian random variable whose variance is a function of the σ^0 value. Thus, $\nu \sim N(0, \sqrt{\alpha + (\beta/\sigma^0) + (\gamma/(\sigma^0)^2)})$, where $\alpha = 0.0025$, $\beta = 1.9 \times 10^{-4}$, and $\gamma = 1.2 \times 10^{-7}$ [4]. σ^0 fields are simulated for various rain rates, and the error of the resulting wind fields is calculated. Ideal ambiguity selection (the conventional high-resolution ambiguity closest to the H*Wind), MAP ambiguity selection, and MAP estimation are compared. For simulation, the MAP ambiguity selection and MAP estimation eye centers are fixed to the true eye center.

Fig. 7 shows the rms error versus rain rate averaged over a few H*Wind fields used in simulation. On average, the MAP estimation procedure reduces the rms error lower than even ideal ambiguity selection (and thus does much better than the conventional ambiguity selection). Also, MAP ambiguity selection approaches ideal ambiguity selection in the rms error sense. These results suggest that, for all rain rates, the MAP estimation procedure is superior to the other methods and that

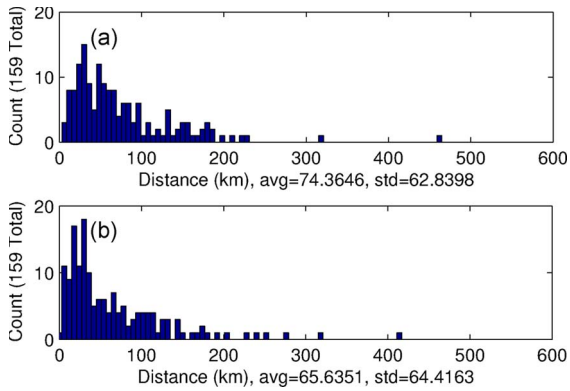

Fig. 8. Histogram of the distance of eye center from best track location for (a) the model fit method and (b) the CHT method. Results are derived from 159 North Atlantic named storms from 1999 to 2005.

the MAP ambiguity selection method is similar to ideal ambiguity selection and, thus, generally better than the conventional approach.

B. Quality of the Hurricane Model Parameters

This section analyzes the scatterometer-derived hurricane model parameters: the eye center estimates, the maximum speed scale factor, and the mean flow. The eye center results are compared with the best track locations (which are interpolated to the same time as the QuikSCAT measurements). First, the MAP ambiguity selection eye center location, which is derived from the hurricane model fit, is evaluated. Next, the CHT eye finding method is analyzed. Then, the conventional high-resolution method is explored with respect to the eye center parameter. Because the conventional high-resolution method provides no eye location estimate, the conventional eye location is estimated from the vector field and compared with the results of the other methods (CHT and hurricane model fit). The maximum speed scale factor and the mean flow parameters are then compared to maximum wind speed and mean flow quantities derived from NCEP winds.

The best track locations are compared to the new eye location derived from the hurricane model fit. Fig. 8(a) shows the histogram of the distance between the best track eye locations and the eye locations derived by using only the hurricane model for a number of observations of North Atlantic storms from 1999 to 2005. The mean and standard deviation are reported as well. The distribution shows that the majority of cases are at low distance bins but the mean and standard deviation are quite large. This can be due to several factors such as rain contamination, unmodeled parameters, swath edge effects, land contamination, and including underdeveloped storms in the analysis.

The eye center locations from the CHT method are compared to the best track locations provided by the NHC. The mean and standard deviation of the distance from the interpolated best track location are also calculated for the eye center found by the CHT method. Fig. 8(b) shows the histogram of the distance from the best track eye center for the CHT method for the same hurricanes as in Fig. 8(a). The mean is improved over the method that uses only the model fit to find the eye.

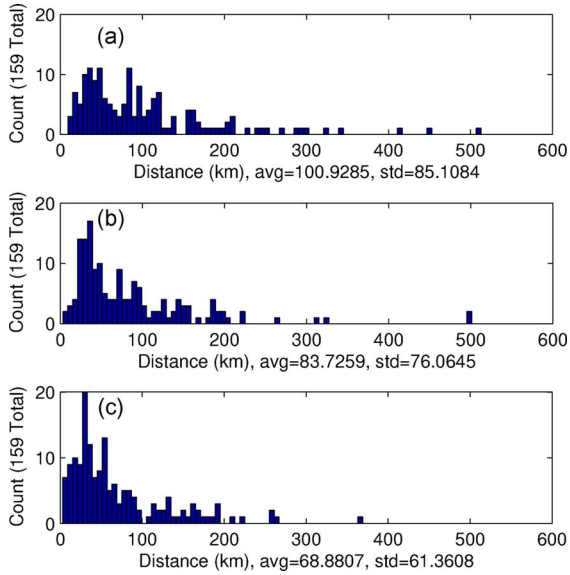

Fig. 9. Histogram of the distance of eye center from best track location for (a) the conventional high-resolution method, (b) the fieldwise MAP wind method, and (c) the CHT method all based on the curl of the vector fields. The same storms as in Fig. 8 are used.

In order to compare the methods with the conventional approach, the eye centers are estimated by using the curl of the vector fields. Fig. 9 shows the distributions for distance from the best track for the conventional high-resolution eye, the fieldwise MAP eye, and the CHT eye based on the curl of the vector fields. The mean and standard deviations of the fieldwise MAP and CHT eyes are lower than the those corresponding to the conventional eye, suggesting that both new methods generally perform better than the conventional method.

The new eye finding method based on the CHT generally improves the eye estimates over the conventional method; however, a human can improve the results even further. Because hurricanes are relatively rare, using human analysts for eye finding is a feasible alternative to purely automated data processing. According to [20], a human in the loop can improve the average error from the best track to 21.1 km. However, some storm observations must be discarded in the analysis because the eye center is not obvious to a human. Furthermore, human-based analysis is somewhat subjective. A fully automated method, such as the CHT method, provides objective and timely results.

We analyze the quality of the other estimated hurricane model parameters (the maximum speed scale factor and the mean flow) using NCEP winds as reference. For both the maximum speed scale factor and the mean flow analysis, we manually fix the eye center estimates. First, we compare the estimated maximum speed scale factor to the maximum wind speed reported by the spatially interpolated NCEP wind field. Fig. 10(a) shows the scatter plot of the maximum speed scale factor versus the maximum NCEP wind speed of several different QuikSCAT observations of hurricanes. The general correlation between the two quantities suggests that the maximum speed scale factor estimates are consistent with the NCEP maximum speed.

We compare the estimates of the mean flow to a mean flow quantity derived from the NCEP winds. The NCEP mean flow

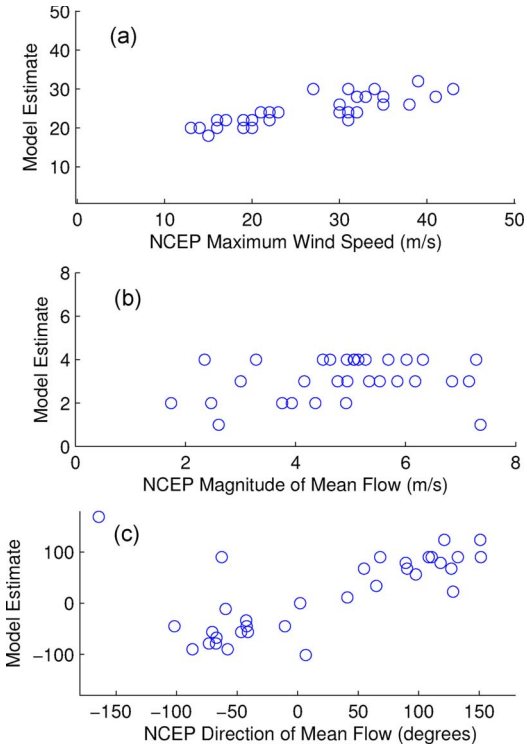

Fig. 10. Scatter plot of the hurricane model estimates versus corresponding NCEP-derived quantities. (a) Maximum speed scale factor. (b) Magnitude of mean flow. (c) Direction of mean flow.

is found by taking the vector average of the wind field in the vicinity of the hurricane. Fig. 10(b) shows the scatter plot of the magnitude of the mean flow estimate derived from QuikSCAT versus the magnitude of the NCEP mean flow. Whereas the correlation is somewhat weak, the quality of the wind estimates is not particularly sensitive to errors in the magnitude of the mean flow. Fig. 10(c) shows the scatter plot of the direction of mean flow derived from QuikSCAT versus the NCEP direction of mean flow. The two parameters correlate well, suggesting that the MAP ambiguity selection algorithm estimates the direction of the mean flow relatively well.

C. Accuracy of the Estimated Winds

In order to test the quality of the estimated winds, we use the standard H*Wind products. The H*Wind fields are smoothed over several hours and do not exhibit much of the small-scale information that exists in the QuikSCAT UHR fields. Nevertheless, we use H*Winds to compare to the new wind estimates because the H*Winds are readily available, commonly used in hurricane analysis, and useful for studying the larger scale storm structure [7].

The scatterometer-derived winds are compared to the closest (in time and space) H*Winds for a typical storm observation (Hurricane Isabel 2003). We compare the conventional high-resolution winds, the MAP ambiguity selection, and the MAP estimates to the H*Winds and calculate several metrics. Table II reports the vector rms difference, the mean and standard deviation of the speed difference, and the mean and standard deviation of the direction difference for the three wind estimation schemes. The MAP ambiguity selection method

TABLE II
DIFFERENCES FROM H*WINDS FOR THE CONVENTIONAL, MAP AMBIGUITY SELECTION, AND MAP ESTIMATION METHODS FOR THE OBSERVATION OF HURRICANE ISABEL 2003

	Conventional UHR	MAP Ambsel	MAP Estimate
Vector RMS	17.19 m/s	14.60 m/s	10.15 m/s
Speed Mean	4.47 m/s	4.35 m/s	3.90 m/s
Speed Std	6.57 m/s	6.43 m/s	5.31 m/s
Dir Mean	-13.15 deg.	-0.28 deg.	5.65 deg.
Dir Std	42.27 deg.	33.31 deg.	20.51 deg.

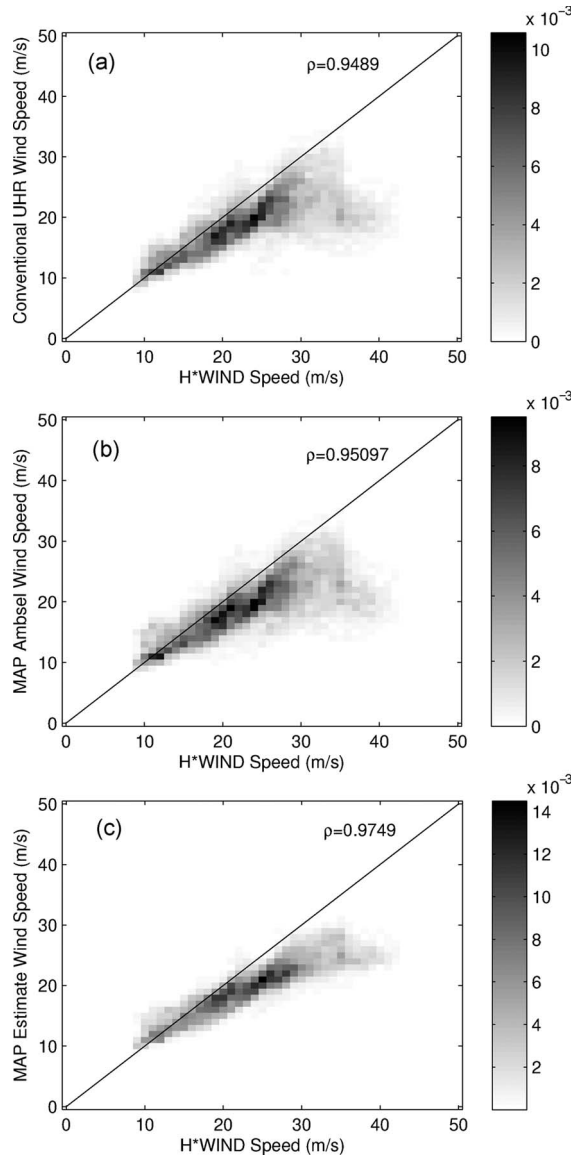

Fig. 11. Density plots of the H*Wind wind speed versus the scatterometer wind speeds from the three wind retrieval schemes for the observation of Hurricane Isabel 2003. (a) Conventional UHR. (b) MAP ambiguity selection. (c) MAP estimation. The correlation coefficients are also reported.

improves the rms difference and the speed and direction standard deviations over the conventional method, and the MAP estimate improves these same quantities over the MAP ambiguity selection method. This suggests that the MAP estimation procedure produces results that are more consistent with the standard H*Wind products.

Fig. 11 shows the density plots of the H*Wind wind speed versus the scatterometer winds for the three wind retrieval

schemes for the same observation of Hurricane Isabel. The correlation coefficient (ρ) is also reported. The correlation coefficients for each of the methods are very high but the MAP estimation winds are the highest. This implies that an affine transformation of the MAP estimated wind field is most consistent with the H*Wind field. Note that the general trend of the data is linear with a slope less than one and intercept greater than zero. Applying bias correction (augmenting the retrieved wind speeds so that the slope is one and the intercept is zero) may make the scatterometer data more consistent with the H*Winds. Alternatively, improving the GMF for hurricanes (particularly the high wind speeds which tend to be underestimated with the current GMF) may improve the consistency with H*Winds. Nevertheless, in the upper right portion of the images (the high wind speed region), the variance of the data is significantly reduced with the MAP estimation scheme. This suggests that the MAP estimation procedure produces a less noisy (although still biased) estimate of the high wind speeds as compared with H*Winds for this storm observation.

Fig. 12 shows an example of a real storm (Floyd 1999). Conventional wind retrieval, fieldwise MAP ambiguity selection, and fieldwise MAP wind retrieval are all shown. Using the MAP model reduces the variability of the speed and direction estimates, which gives the illusion of biasing low the wind speed compared to the nonmodel-based ML estimates. The MAP ambiguity selection routine finds the eye center better than the conventional method and improves the ambiguity selection. The lower left quadrant of the storm where the vectors are pinned in the cross-track direction in the conventional high-resolution product due to rain contamination are corrected in the MAP ambiguity selection and MAP estimation products. The fieldwise MAP wind retrieval method produces a more smooth and less squared off storm than even the fieldwise MAP ambiguity selection. This suggests that the MAP estimation procedure may mitigate the directional biases of conventional wind retrieval (which account for some of the squaring off of the storms even in nonraining portions of the storms). Although MAP estimation utilizes a model that does not describe the comma cloud and smaller convective events (speckles in the wind speed image), the MAP estimation method reports a similar speed field structure as the conventional (nonmodel-based) method.

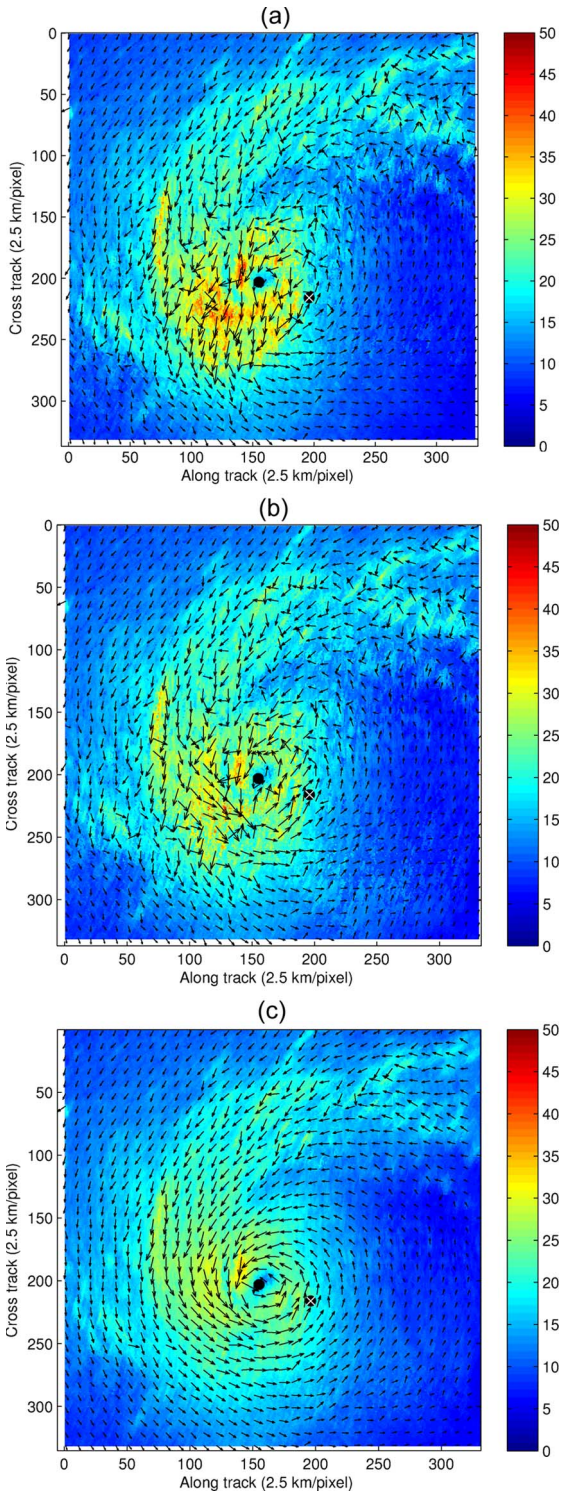

Fig. 12. Hurricane Floyd (1999) example. (a) Conventional UHR wind field. (b) Result of the fieldwise MAP ambiguity selection. (c) Fieldwise MAP estimate of the wind field. The wind vector fields are down sampled by ten for plotting. The black dots represent the eye center reported by the new method, and the black dots with white x's represent the conventional high-resolution eye center based on the curl of the vector field. The smoothness of the MAP estimate may be adjusted by scaling the variances of the priors. The MAP estimation uses the variances suggested by the empirical priors.

VII. Conclusion

The fieldwise MAP wind retrieval method presented can be used to augment scatterometer hurricane analysis. It reduces the variability of the wind vector estimates, provides estimates of useful hurricane parameters (such as the eye center location), and improves wind direction estimates—particularly in rain-contaminated portions of the storm. Furthermore, the method can be applied in near real time.

The hurricane model is simplistic but appropriate for MAP techniques in well-developed tropical cyclones. Moreover, the MAP procedure allows the operator to vary how much the model is imposed.

MAP estimation mitigates the effects of noise and rain but relies on a hurricane model fit to generate appropriate prior distributions. Although the new method imposes a low-order model, the effects are less severe than pure model-based methods as the MAP estimation scheme preserves small-scale information that is not represented by the model.

MAP ambiguity selection provides an improved selection of the ML ambiguities in tropical cyclones. Although rain and noise artifacts remain in the result, MAP ambiguity selection imposes the model more weakly than MAP estimation and even standard nudging. Therefore, MAP ambiguity selection may be more appropriate than MAP estimation for certain applications (such as the study of smaller scale structures on the order of 3–10 km).

Simulation suggests that where an eye center can be found in the data, the MAP estimation and ambiguity selection methods are superior to the conventional high-resolution approach for all realistic rain rates. The eye center location for the new method is improved over the conventional method (using the curl of the vector fields). However, the eye center estimates may be improved further by a human analyst. Furthermore, the MAP estimation procedure produces results that are more consistent with the standard H*Wind product, although the wind speed estimates tend to remain underestimated compared to H*Winds due to the GMF and rain contamination. The method may be further improved by using quality control and an improved GMF for hurricane conditions (high wind speeds and rain rates).

Future work will include the development of quality control algorithms and simultaneous wind and rain estimation in hurricanes. We will also consider a wind and rain field model for simultaneous wind and rain MAP estimation. Future work will also explore MAP nudging (pointwise MAP ambiguity selection with NWP winds as the mean of the prior), which can be applied to generic wind structures beyond tropical cyclones. The MAP procedure assumes that a hurricane is present in the data. Future research will involve the use of the MAP model with automatic hurricane detection.

ACKNOWLEDGMENT

The authors would like to thank the Jet Propulsion Laboratory for providing the QuikSCAT data through the PO.DACC and the NOAA Hurricane Research Division of the Atlantic Oceanographic and Meteorological Laboratory for providing the H*Wind products.

REFERENCES

[1] D. G. Long, "High resolution wind retrieval from SeaWinds," in *Proc. IGARSS*, 2002, pp. 751–753.
[2] D. G. Long, J. B. Luke, and W. Plant, "Ultra high resolution wind retrieval from SeaWinds," in *Proc. IGARSS*, 2003, pp. 1264–1266.
[3] S. H. Yueh, B. W. Stiles, W.-Y. Tsai, H. Hu, and W. T. Liu, "QuikSCAT geophysical model function for tropical cyclones and application to Hurricane Floyd," *IEEE Trans. Geosci. Remote Sens.*, vol. 39, no. 12, pp. 2601–2612, Dec. 2001.
[4] T. Lungu, *QuikSCAT Science Data Product Users Manual Overview and Geophysical Data Products*, Sep. 2006.
[5] N. Suzuki, M. A. Donelan, and W. J. Plant, "On the sub-grid-scale variability of oceanic winds and the accuracy of numerical weather prediction models as deduced from QuikSCAT backscatter distributions," *J. Geophys. Res.*, vol. 112, no. C4, p. C04 005, 2007.
[6] M. Portabella and A. Stoffelen, "Scatterometer backscatter uncertainty due to wind variability," *IEEE Trans. Geosci. Remote Sens.*, vol. 44, no. 11, pp. 3356–3362, Nov. 2006.
[7] M. D. Powell, S. H. Houston, L. R. Amat, and N. Morisseau-Leroy, "The HRD real-time hurricane wind analysis system," *J. Wind Eng. Ind. Aerodyn.*, vol. 77/78, pp. 53–64, 1998.
[8] M. W. Spencer, C. Wu, and D. G. Long, "Tradeoffs in the design of a spaceborne scanning pencil beam scatterometer: Application to SeaWinds," *IEEE Trans. Geosci. Remote Sens.*, vol. 35, no. 1, pp. 115–126, Jan. 1997.
[9] S. J. Shaffer, R. S. Dunbar, S. V. Hsiao, and D. G. Long, "A median-filter-based ambiguity removal algorithm for NSCAT," *IEEE Trans. Geosci. Remote Sens.*, vol. 29, no. 1, pp. 167–174, Jan. 1991.
[10] B. W. Stiles, B. D. Pollard, and R. S. Dunbar, "Direction interval retrieval with thresholded nudging," *IEEE Trans. Geosci. Remote Sens.*, vol. 40, no. 1, pp. 79–89, Jan. 2002.
[11] W. J. Pierson, Jr., "Probabilities and statistics for backscatter estimates obtained by a scatterometer," *J. Geophys. Res.*, vol. 94, no. C7, pp. 9743–9759, Jul. 1989.
[12] A. C. Lorenc, "Analysis methods for numerical weather prediction," *Q. J. R. Meteorol. Soc.*, vol. 112, no. 474, pp. 1177–1194, 1986.
[13] M. Portabella and A. Stoffelen, "A probabilistic approach for SeaWinds data assimilation," *Q. J. R. Meteorol. Soc.*, vol. 130, no. 596, pp. 127–152, 2004.
[14] A. Stoffelen and M. Portabella, "On Bayesian scatterometer wind inversion," *IEEE Trans. Geosci. Remote Sens.*, vol. 44, no. 6, pp. 1523–1533, Jun. 2006.
[15] C. Mears, D. Smith, and F. Wentz, "Detecting rain with QuikSCAT," in *Proc. IGARSS*, 2000, pp. 1235–1237.
[16] D. W. Draper and D. G. Long, "Evaluating the effect of rain on SeaWinds scatterometer measurements," *J. Geophys. Res.*, vol. 109, no. C2, p. C02 005, 2004.
[17] J. N. Huddleston and B. W. Stiles, "A multidimensional histogram rain-flagging technique for SeaWinds on QuikSCAT," in *Proc. IGARSS*, 2000, vol. 3, no. 24–28, pp. 1232–1234.
[18] M. Portabella and A. Stoffelen, "Characterization of residual information for SeaWinds quality control," *IEEE Trans. Geosci. Remote Sens.*, vol. 40, no. 12, pp. 2747–2759, Dec. 2002.
[19] D. W. Draper and D. G. Long, "Simultaneous wind and rain retrieval using SeaWinds data," *IEEE Trans. Geosci. Remote Sens.*, vol. 42, no. 7, pp. 1411–1423, Jul. 2004.
[20] R. R. Halterman and D. G. Long, "A comparison of hurricane eye determination using standard and ultra-high resolution QuikSCAT winds," in *Proc. IGARSS*, 2006, pp. 4134–4137.

Brent A. Williams (S'04–M'08) received the B.S. degree in electrical engineering from Brigham Young University, Provo, UT, in 2005, where he is currently working toward the Ph.D. degree in electrical engineering at the Electrical and Computer Engineering Department.

Since 2005, he has been with the Microwave Earth Remote Sensing Laboratory exploring ultrahigh resolution (UHR) ocean wind scatterometry. His current research interests are in the estimation, ambiguity removal, and validation of UHR wind fields derived from the SeaWinds scatterometer.

Mr. Williams is a member of Eta Kappa Nu.

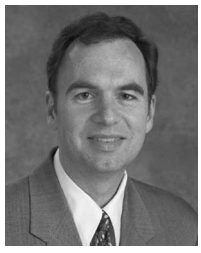

David G. Long (S'80–M'82–SM'98–F'07) received the Ph.D. degree in electrical engineering from the University of Southern California, Los Angeles, in 1989.

From 1983 to 1990, he was with the Jet Propulsion Laboratory (JPL), National Aeronautics and Space Administration (NASA), where he developed advanced radar remote sensing systems. While at JPL he was the Project Engineer on the NASA Scatterometer (NSCAT) project, which flew from 1996 to 1997. He also managed the SCANSCAT project, the precursor to SeaWinds, which was launched in 1999 and 2002. He is currently a Professor with the Department of Electrical and Computer Engineering, Brigham Young University, Provo, UT, where he teaches upper-division and graduate courses in communications, microwave remote sensing, radar, and signal processing, and is the Director of the BYU Center for Remote Sensing. He is the Principal Investigator on several NASA-sponsored research projects in remote sensing. He is the author or coauthor of more than 275 publications in signal processing and radar scatterometry. His research interests include microwave remote sensing, radar theory, space-based sensing, estimation theory, signal processing, and mesoscale atmospheric dynamics.

Dr. Long is an Associate Editor of the IEEE GEOSCIENCE AND REMOTE SENSING LETTERS. He has received the NASA Certificate of Recognition several times.